Earth and Planetary Science Letters 412 (2015) 235–244

Contents lists available at ScienceDirect

Earth and Planetary Science Letters

www.elsevier.com/locate/epsl

Dead Sea drawdown and monsoonal impacts in the Levant during the last interglacial

Adi Torfstein [a,b,c,*], Steven L. Goldstein [a,d], Yochanan Kushnir [a], Yehouda Enzel [b], Gerald Haug [e], Mordechai Stein [f]

[a] Lamont-Doherty Earth Observatory of Columbia University, 61 Rt. 9W, Palisades, NY 10964, USA
[b] Institute of Earth Sciences, Hebrew University of Jerusalem, Jerusalem 91904, Israel
[c] Interuniversity Institute of Marine Sciences, Eilat 88103, Israel
[d] Department of Earth and Environmental Sciences, Columbia University, 61 Rt. 9W, Palisades, NY 10964, USA
[e] ETH Zürich, Geologisches Institut, NO G 51.1, Sonneggstrasse 5, 8092 Zürich, Switzerland
[f] Geological Survey of Israel, 30 Malkhe Israel Street, Jerusalem 95501, Israel

ARTICLE INFO

Article history:
Received 7 August 2014
Received in revised form 29 November 2014
Accepted 4 December 2014
Available online 9 January 2015
Editor: J. Lynch-Stieglitz

Keywords:
last interglacial
paleoclimate
Dead Sea
sapropel
Levant
African monsoon

ABSTRACT

Sediment cores recovered by the Dead Sea Deep Drilling Project (*DSDDP*) from the deepest basin of the hypersaline, terminal Dead Sea (lake floor at ~725 m below mean sea level) reveal the detailed climate history of the lake's watershed during the last interglacial period (Marine Isotope Stage 5; MIS5). The results document both a more intense aridity during MIS5 than during the Holocene, and the moderating impacts derived from the intense MIS5e African Monsoon. Early MIS5e (~133–128 ka) was dominated by hyperarid conditions in the Eastern Mediterranean–Levant, indicated by thick halite deposition triggered by a lake-level drop. Halite deposition was interrupted however, during the MIS5e peak (~128–122 ka) by sequences of flood deposits, which are coeval with the timing of the intense precession-forced African monsoon that generated Mediterranean sapropel S5. A subsequent weakening of this humidity source triggered extreme aridity in the Dead Sea watershed and resulting in the biggest known lake level drawdown in its history, reflected by the deposition of thick salt layers, and a capping pebble layer corresponding to a hiatus at ~116–110 ka. The *DSDDP* core provides the first evidence for a direct association of the African monsoon with mid subtropical latitude climate systems effecting the Dead Sea watershed. Combined with coeval deposition of Arabia and southern Negev speleothems, Arava travertines, and calcification of Red Sea corals, the evidence points to a climatically wet corridor that could have facilitated *homo sapiens* migration "out of Africa" during the MIS5e peak. The hyperaridity documented during MIS5e may provide an important analogue for future warming of arid regions of the Eastern Mediterranean–Levant.

1. Introduction

The Dead Sea is a hypersaline, terminal lake occupying the lowest surface on Earth's continents, whose water surface is currently at ~428 m below mean sea level (mbsl), and whose large (~40 000 km^2) watershed spans the Mediterranean and the Saharo–Arabian climate zones (Fig. 1). Its volume increases during glacials and declines during interglacials, with amplified positive and negative responses of its levels, respectively. The mineralogy, grain sizes, and chemical and isotope compositions of the lake deposits reflect the regional climate during past glacial-interglacial cycles (Enzel et al., 2008; Stein, 2001). Studies of the Holocene Dead Sea, the last glacial Lake Lisan, and earlier Pleistocene lake cycles (i.e., Lake Amora), based mainly on exposed deposits along the lake margins, show close connections between Northern Hemisphere (NH) climate changes and water levels, water chemistry, and sediment lithology on glacial-interglacial to millennial time-scales (Bartov et al., 2003; Haase-Schramm et al., 2004; Kushnir and Stein, 2010; Prasad et al., 2004; Torfstein et al., 2013b). For example, since the Last Glacial Maximum and during the last deglaciation (~24–11 ka), lake level dropped from its glacial high-stand of ~160 mbsl to below 460 mbsl at the Bølling–Allerød (Stein et al., 2010), stabilizing at a Holocene (average) level of ~400 mbsl. However, margin exposures cover limited time-intervals and mainly sediments deposited during the last glacial Lake Lisan (e.g., Bartov et al., 2002); continuous sedimentation

* Corresponding author at: Institute of Earth Sciences, Hebrew University of Jerusalem, Jerusalem 91904, Israel.
E-mail address: adi.torf@mail.huji.ac.il (A. Torfstein).

http://dx.doi.org/10.1016/j.epsl.2014.12.013
0012-821X/

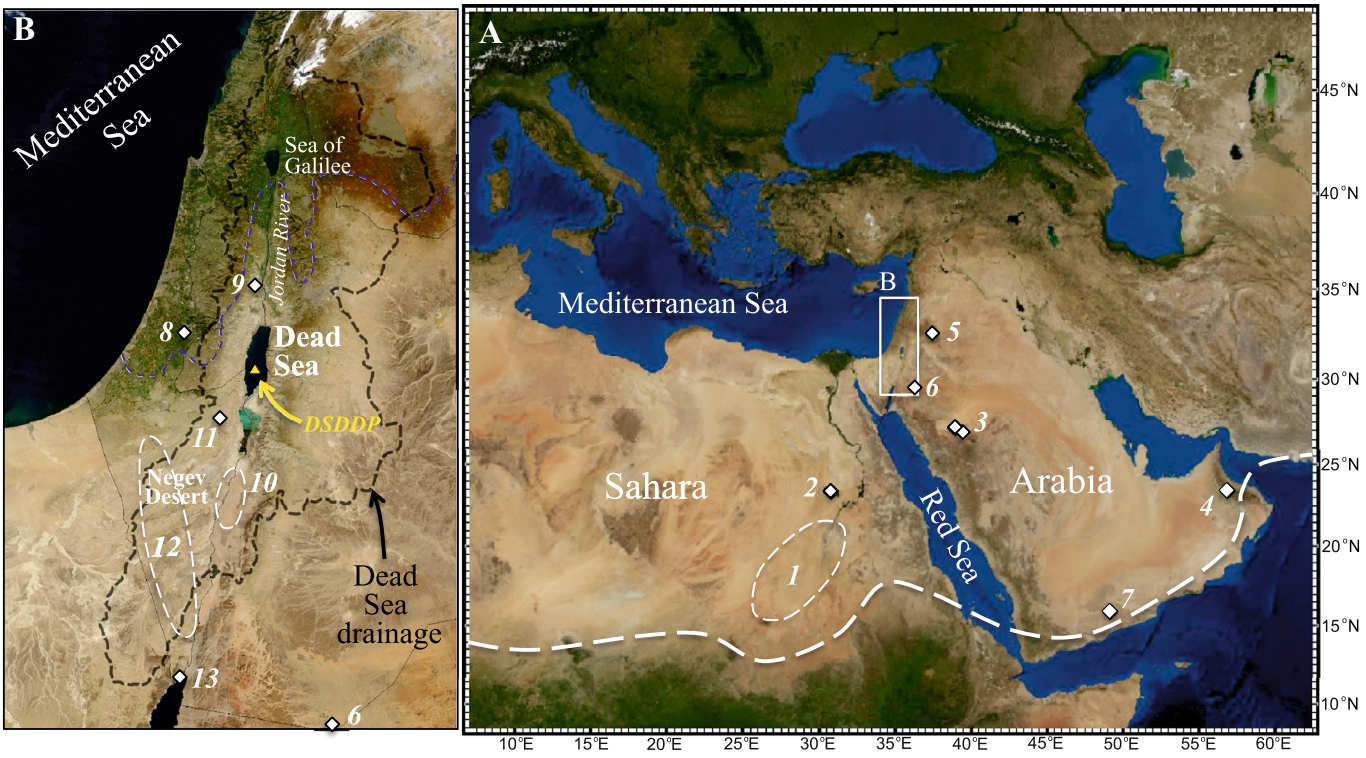

Fig. 1. (A) Regional location map. The Dead Sea basin is located between the Saharo–Arabia desert belt and the Mediterranean climate zone. The modern northern boundary of the boreal summer rains is marked by a thick-dashed white curve. (B) The Dead Sea watershed. The lake receives waters from a large watershed encompassing the two above mentioned climate zones, and its composition and sedimentary record reflect the climate-hydrological conditions over a very large geographical area. A dashed blue line marks the approximate locus of the 400 mm/y isohyet beyond which a steep climate gradient leads to an extreme desert environment. Currently, most of the precipitation in the northern Dead Sea watershed comes the Mediterranean during the winter. The Negev Desert and Arava valley in the southern part of the watershed receive minor amounts of localized rain primarily associated with active Red Sea trough systems and tropical plumes (Ziv et al., 2006). During the last interglacial the areas that currently receive rains from east Mediterranean sources were significantly drier. Locations of geological archives discussed in this paper: The *DSDDP* core location at the mid-Dead Sea; Then (by numbers): (1) Northern Sahara (Smith et al., 2007; Szabo et al., 1995); (2) Western Desert–Egypt (Crombie et al., 1997); (3) Nafud Desert (Rosenberg et al., 2013); (4) Oman Cave (Fleitmann et al., 2003); (5) Azraq Oasis–Jordan (Cordova et al., 2013); (6) South Jordan (Petit-Maire et al., 2010); (7) Yemen Cave (Fleitmann et al., 2011); (8) Soreq Cave (Bar-Matthews, 2014; Bar-Matthews et al., 2003); (9) Ma'ale Efrayim Cave (Vaks et al., 2003); (10) Arava valley travertines (Livnat and Kronfeld, 1985; Waldmann et al., 2010); (11) Tzavo'a Cave (Vaks et al., 2006); (12) Central and Southern Negev Caves (Vaks et al., 2007); (13) Gulf of Aqaba corals (Lazar and Stein, 2011).

has occurred only in the deepest part of the lake. The Dead Sea Deep Drilling Project (*DSDDP*) conducted in 2010–2011 under the auspices of the Intercontinental Scientific Drilling Program (*ICDP*), recovered a detailed sedimentary record going back to MIS7, from the deepest basin of the modern lake (Neugebauer et al., 2014). The drilling took place at a lake depth of 297 m, and the coring reached 456 m below the lake floor (mblf), recovering otherwise hidden sedimentary sections of the last interglacial low-stand lake.

This study presents a 200 kyr climate record from the DSDDP core and focuses on the climate history of the Levant during the last interglacial MIS5. This time interval has relevance in the context of climate models indicating a more arid Middle East with increasing global temperatures (e.g., Held and Soden, 2006), thus implying increased future fresh water scarcity in a water-starved and politically unstable region. Because the last interglacial peak (MIS5e, between ~135–116 ka; Lisiecki and Raymo, 2005) was characterized by stronger insolation, warmer global temperatures, higher sea levels, and smaller continental ice sheets compared to the Holocene, the DSDDP core record provides a test of such predictions; thus, it serves as an analogue for a future warmer world. Our results show both extreme hyperaridity during MIS5e, including an unprecedented drawdown of Dead Sea water levels, as well as important impacts of a particularly strong precession-controlled African monsoon that generated a major sapropel (S5; Rohling et al., 2002; Rossignol-Strick, 1985) in the eastern Mediterranean.

2. Sedimentary records of the Dead Sea lakes and their hydroclimate connection

Previous studies on marginal terraces and short cores drilled along the Dead Sea shores have revealed that the lithology of the lacustrine sections directly reflects the watershed hydroclimatology (e.g., Begin et al., 1974; Bookman (Ken-Tor) et al., 2004; Haase-Schramm et al., 2004; Migowski et al., 2006; Stein et al., 1997; Yechieli et al., 1993). A wet hydrological regime is represented by summer deposition of primary (evaporitic) aragonitic laminae. These laminae alternate with detrital quartz and calcite silt grains from desert dust origin (Haliva-Cohen et al., 2012), that accumulated in the Dead Sea watershed and was washed into the lake during winters. The alternating aragonite and detritus couplets comprising the *aad facies* (Figs. 2, S1) reflect annual cycles of deposition (Begin et al., 1974; Prasad et al., 2004). The Ca-chloride Dead Sea brine is poor in bi-carbonate and sulfate, required for aragonite or gypsum precipitation. These ions are supplied by freshwaters entering the lake during wet periods in the watershed, and support the precipitation of aragonite and gypsum, which are characteristic of wet glacial intervals in the Dead Sea lacustrine deposits (Stein et al., 1997; Torfstein et al., 2008, 2005). During arid periods, smaller amounts of bicarbonate and sulfate are supplied to the lake and the deposition is dominated the silty quartz and calcite grains comprising the laminated detritus (the *ld facies*; Haliva-Cohen et al., 2012). This sediment comprises significant portions of the interglacial sequences exposed along the margins of the modern lake (e.g.,

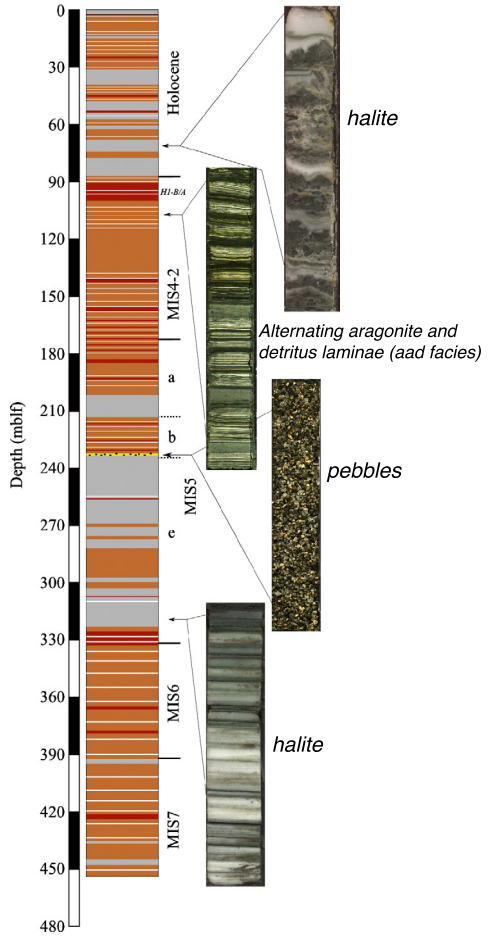

Fig. 2. Compiled columnar section and primary sedimentary facies. The main types of sediments comprising the DSDDP core are: (1) Alternating aragonite and detritus laminae (*aad facies*; brown-white lamination), characterizing periods of enhanced freshwater input; (2) Laminated silts (*ld facies*; brown), characterizing floods occurring during periods of relative aridity; (3) Halite (gray) and gypsum layers (red) marking lake level drops. A pebble unit ca. 235 mblf (yellow) marks the catastrophic low point of water elevations during MIS5. (For interpretation of the references to color in this figure legend, the reader is referred to the web version of this article.)

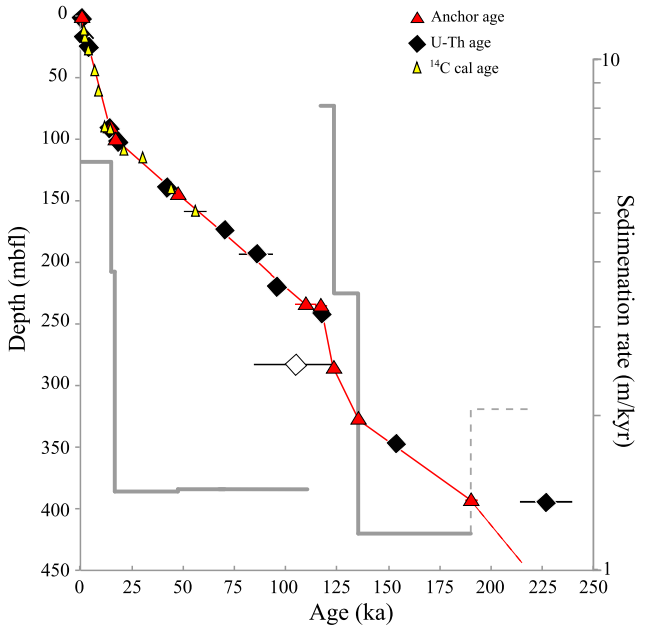

Fig. 3. Age model and sedimentation rates. Anchor ages (red triangles) were determined based on the compilation of U–Th ages, correlation of defined stratigraphic layers to well dated counterparts on the basins margins, and a fit between the oxygen isotope stratigraphy and main lithological facies to the LR04 (Lisiecki and Raymo, 2005) and Soreq Cave (Bar-Matthews et al., 2003; Grant et al., 2012) records (details in Supplementary Material). The sedimentation rates show large variations, whereby glacial and interglacial stages are characterized by low and high rates, respectively. Radiocarbon ages of organic material in the DSDDP core (yellow triangles) are from Neugebauer et al. (2014). (For interpretation of the references to color in this figure legend, the reader is referred to the web version of this article.)

the Amora/Samra and early Holocene Formations; Migowski et al., 2006; Torfstein et al., 2009; Waldmann et al., 2009). Increasing aridity in the watershed is reflected by the deposition of gypsum, and hyperaridity along with significant lake level drops is reflected by deposition of halite. Thick sequences of halite have been recovered during shallow drilling along the Dead Sea margins to the base of the Holocene (Neev and Emery, 1967; Stein et al., 2010; Yechieli et al., 1993).

3. U–Th ages and age model

U–Th ages were obtained on primary aragonites that comprise thin laminae of the *aad* facies throughout the core. Analytical procedures are summarized in the Supplementary Material. The approach to achieve U–Th (calendar) ages from the primary aragonites of the late Quaternary Dead Sea lacustrine sections was developed over several decades of research (Haase-Schramm et al., 2004; Kaufman, 1971; Kaufman et al., 1992; Schramm et al., 2000; Torfstein et al., 2013a). The Dead Sea aragonites have been called "dirty carbonates" because they contain some detrital Th and U, and hydrogenous Th, all requiring the appropriate corrections to the simple age equation. Here, we estimated the U and Th concentrations and isotope compositions of the Detritus End Member (DEM) for each individual set of coeval samples. This was based on the intercept between the extrapolated ($^{234}U/^{238}U$)–($^{230}Th/^{238}U$)–($^{232}Th/^{238}U$) ratios of the samples and the secular equilibrium curve, under the premise that ^{238}U, ^{234}U and ^{230}Th are in secular equilibrium in detritus material (details in Torfstein et al., 2013a). The extracted DEM value is subsequently used to correct the individual sample ages (i.e., 'single sample ages'), with an assumed (conservative) uncertainty of 30%, according to procedures described in Haase-Schramm et al. (2004) and Torfstein et al. (2013a). Because the impact of a potential hydrogenous Th component is limited to several hundreds of years and is negligible in samples older than several tens of thousands of years, we do not consider this component in the calculations. The measured ratios, and the calculated ages are listed in Table 1.

The age-depth model for the *DSDDP* core (Fig. 3; Table 2) is based on the integration of the U–Th ages with oxygen isotope ratios in aragonite from the core, and lithological changes in the core, all of which are tied to key points in the LR04 and Soreq Cave $\delta^{18}O$ records (Bar-Matthews et al., 2003; Grant et al., 2012; Lisiecki and Raymo, 2005), as well as correlations between distinct stratigraphic units to well-dated counterparts on the exposed margins of the Dead Sea basin (details in Supplementary Material).

4. Chronology and stratigraphy of the DSDDP MIS5 interval

From the *DSDDP* core litho-stratigraphy, a first order observation is that glacial terminations and interglacials are characterized by halite, gypsum, and laminated silt clastics (Fig. 2). The glacial intervals display thick sequences of the *aad facies* with some gypsum and silts during drier intervals (Fig. 2). Here, we focus on the last interglacial MIS5 interval (328–177 mblf), comprising thick halite sequences interspersed with intermittent gypsum, sequences of silt layers, and some sequences of the *aad facies*. As already noted, these lithologies document major climatic shifts ranging

Table 1
U–Th data. Ages used for age model construction are highlighted in bold font. Rounded brackets mark activity ratios.

Sample name	Depth (m)	(^{230}Th/^{238}U)	2σ	(^{234}U/^{238}U)	2σ	(^{230}Th/^{232}Th)	2σ	U (ppm)	Th (ppm)	^{232}Th/^{238}U (atomic) detritus correction	Single sample age (y)	2σ (+)	2σ (−)	Isochron age (y)	2σ (+)	2σ (−)	Average single sample age (y)	2σ stderr
AT-105-d	2.76	0.190	4.1E−04	1.420	7E−04	2.12	4E−03	1.30	0.355	1.539	673	80	73	**−64**	150	−66	906	466
AT-105-e	2.76	0.278	7.1E−04	1.379	8E−04	2.13	5E−03	1.75	0.701	1.539	1139	221	187					
AT-47-d	16.94	0.415	9.3E−04	1.341	1E−03	2.77	5E−03	2.13	0.970	1.381	8478	2426	1867	**1858**	1909	1769	4727	3834
AT-47-c	16.94	0.240	5.6E−04	1.421	8E−04	2.52	6E−03	1.61	0.467	1.381	2167	306	269					
AT-47-b	16.94	0.173	4.0E−04	1.429	1E−03	2.98	7E−03	0.73	0.130	1.381	3534	268	249					
AT-1	21.25	0.248	4.5E−04	1.406	1E−03	2.40	4E−03	2.37	0.746	1.447	**2266**	341	296					
AT-62-a	21.25	0.832	9.0E−04	1.376	5E−04	8.18	7E−03	1.75	0.543	1.447	78 297	17 385	13 172					
AT-21-b	92.20	0.225	4.1E−04	1.467	1E−03	7.00	1E−02	1.97	0.194	1.447	12 813	491	473	**14 067**	1146	1135	12 858	363
AT-21-d	92.20	0.249	6.0E−04	1.467	9E−04	5.78	1E−02	2.68	0.352	1.447	13 036	685	647					
AT-21-e	92.20	0.239	3.7E−04	1.458	9E−04	6.41	9E−03	1.91	0.217	1.447	13 212	589	562					
AT-21-f	92.20	0.244	3.8E−04	1.461	1E−03	5.44	8E−03	2.28	0.312	1.447	12 372	682	643					
AT-28-b	102.10	0.318	5.1E−04	1.407	1E−03	3.86	6E−03	2.95	0.741	2.171	18 149	1295	1198	**18 140**	83	83	18 155	45
AT-28-c	102.10	0.266	4.4E−04	1.437	9E−04	7.24	1E−02	1.82	0.204	2.171	18 119	527	510					
AT-28-d	102.10	0.281	4.8E−04	1.427	8E−04	5.67	9E−03	2.16	0.327	2.171	18 196	711	682					
AT-42-a	139.27	0.507	7.1E−04	1.444	1E−03	13.2	2E−02	1.68	0.197	1.522	40 142	2004	1896	**41 799**	630	630	40 296	935
AT-42-c	139.27	0.508	6.4E−04	1.449	1E−03	14.4	2E−02	1.66	0.178	1.522	40 625	1850	1753					
AT-42-e	139.27	0.539	1.4E−03	1.402	1E−03	7.00	2E−02	2.07	0.487	1.522	39 095	4441	3880					
AT-42-c-dup	139.27	0.513	1.0E−03	1.448	1E−03	14.9	2E−02	1.65	0.173	1.522	41 319	1843	1750					
AT-58-a	174.52	0.763	1.0E−03	1.404	9E−04	8.15	1E−02	1.31	0.376	1.447	65 778	12 128	9642	79 857	4835	4351	**70 513**	4926
AT-58-b	174.52	0.778	1.0E−03	1.417	8E−04	14.3	2E−02	1.31	0.217	1.447	74 057	6954	6124					
AT-58-d	174.52	0.780	4.4E−03	1.317	2E−03	6.66	2E−02	1.29	0.463	1.447	71 704	19 012	13 886					
AT-62-a*	193.58	0.925	1.4E−03	1.389	6E−04	10.6	1E−02	1.00	0.268	1.447	97 006	19 537	14 923	163 531	22 406	18 340	**85 557**	8 176
AT-62-b	193.58	0.837	7.9E−04	1.371	6E−04	7.42	6E−03	1.48	0.509	1.447	77 598	20 020	14 594					
AT-62-c	193.58	0.858	9.3E−04	1.365	7E−04	8.17	7E−03	1.19	0.382	1.447	83 736	20 178	14 885					
AT-62-d (det)	193.58	0.857	1.1E−03	1.367	6E−04	8.41	1E−02	1.22	0.381	1.447	83 889	19 222	14 352					
AT-70-d	220.03	0.841	8.7E−04	1.312	8E−04	15.3	1E−02	3.09	0.517	1.529	96 740	9878	8523	**95 446**	1465	1433	102 205	6481
AT-70-e	220.03	0.850	1.1E−03	1.298	8E−04	11.1	1E−02	2.54	0.595	1.529	96 681	15 215	12 208					
AT-70-f (det)	220.03	0.986	1.9E−03	1.132	7E−04	2.98	4E−03	4.32	4.364	1.529	114 798	362 555	164 606					
AT-74-d	222.91	0.846	9.0E−04	1.339	7E−04	15.1	1E−02	2.27	0.389	1.529	93 970	9709	8402					
AT-70-g	220.03	0.870	8.5E−04	1.302	4E−04	11.0	9E−03	2.29	0.550	1.529	100 146	16 669	13 204					
AT-76-e	241.07	0.993	1.2E−03	1.328	8E−04	9.11	9E−03	1.26	0.420	1.447	118 719	39 470	25 219	120 515	731	732	**117 401**	2637
AT-76-f	241.07	0.981	1.2E−03	1.236	7E−04	4.93	5E−03	2.32	1.405	1.447	116 082	182 787	48 230					
AT-79-e	283.17	0.889	1.0E−03	1.205	6E−04	11.7	1E−02	3.92	0.907	1.149	118 485	32 633	22 183	94 347	14 820	13 345		
AT-79-b	283.17	0.750	9.2E−04	1.222	5E−04	12.6	1E−02	4.31	0.784	1.149	85 237	13 359	10 802					
AT-79-c	283.17	0.948	2.2E−03	1.083	7E−04	3.74	6E−03	5.06	3.917	1.149	109 977	334 134	163 672					
AT-92-c	347.23	1.054	8.8E−04	1.318	6E−04	33.9	2E−02	2.62	0.249	1.447	152 395	11 737	10 238	154 866	2505	2438	**153 837**	981
AT-92-d*	347.23	1.062	1.2E−03	1.321	9E−04	43.6	4E−02	2.55	0.190	1.447	155 333	9176	8259					
AT-92-e	347.23	1.050	9.0E−04	1.304	6E−04	25.8	2E−02	2.73	0.339	1.447	153 513	16 653	13 784					
AT-92-f	347.23	1.054	8.3E−04	1.310	6E−04	28.4	2E−02	2.61	0.296	1.447	153 554	14 851	12 539					
AT-92-g	347.23	1.056	8.2E−04	1.311	8E−04	30.9	2E−02	2.49	0.260	1.447	154 392	13 590	11 632					
AT-97-b	395.00	1.261	4.1E−03	1.302	6E−04	11.3	3E−02	1.59	0.543	1.496	243 534	378 936	78 424	242 587	37 663	27 432	**226 196**	12 957
AT-97-c	395.00	1.236	1.4E−03	1.312	8E−04	22.0	2E−02	1.08	0.186	1.496	228 461	60 967	37 462					
AT-97-e	395.00	1.177	1.3E−03	1.263	7E−04	9.93	9E−03	1.19	0.430	1.496	214 702	221 269	66 828					
AT-97-f	395.00	1.202	1.7E−03	1.290	9E−04	14.3	2E−02	1.18	0.302	1.496	218 087	101 893	48 668					

from hyperarid (reflected by halite deposition) to wetter conditions (reflected by the *aad facies*). We divide the 151 m of MIS5 into six stratigraphic intervals (***I-1*** to ***I-6***) (Figs. 4, 5) reflecting the changing hydrology and climate in the watershed.

Interval I-1 (331–320 mblf, ~137–133 ka) marks the transition from the relatively wet glacial MIS6 to the arid interglacial MIS5e (Termination 2; T2). The ~11 m section comprises gypsum, clastic silts and *aad*. The δ^{18}O of *DSDDP* core aragonites show shifts to lower values, marking the MIS6/5 transition from wet conditions (characterized mainly by *aad* and silt facies) to the arid interglacial conditions. *T*2 marks first major rise in sea level at the end of MIS6 (Grant et al., 2012) and overlaps with Heinrich Event 11 (Hemming, 2004), when the Northern Hemisphere ice sheet breakdown resulted in the discharge of iceberg armadas into the North Atlantic.

Table 2
Age-depth model anchor ages.

Depth (mbif)	Age (ka)
0	0.00 ± 0.20
91	14.50 ± 0.50
101	17.10 ± 0.50
144.5	46.00 ± 1.70
234.6	109.99 ± 5.20
235	116.65 ± 3.00
286.1	123.00 ± 1.00
328	135.00 ± 1.00
393	190.00 ± 3.00
455	220.00 ± 5.00

Interval I-2 (320–303 mblf, ~133–128 ka) marks the initial phase of MIS5, when both high latitude and equatorial summer insolation rise towards their MIS5e peak. The ~17 m section comprises interlayered halite and silty laminae. The aragonite δ^{18}O values are similar to the Holocene (i.e., +2 to +3‰), and both are lower than those of MIS6 (Fig. 4).

Interval I-3 (303–280 mblf, ~128–122 ka) coincides with the peak NH summer insolation during MIS5e. This ~23 m section is mainly comprised of silt layers (Fig. 1), with interspersed aragonite laminae. Despite its coincidence with the peak NH summer insolation and the highest sea level interval of MIS5e, the interval is nearly halite-free (Fig. 4), indicating a temporal dampening of hyperarid conditions and increased wetness in the watershed. It is coeval with anomalously low δ^{18}O values in Soreq

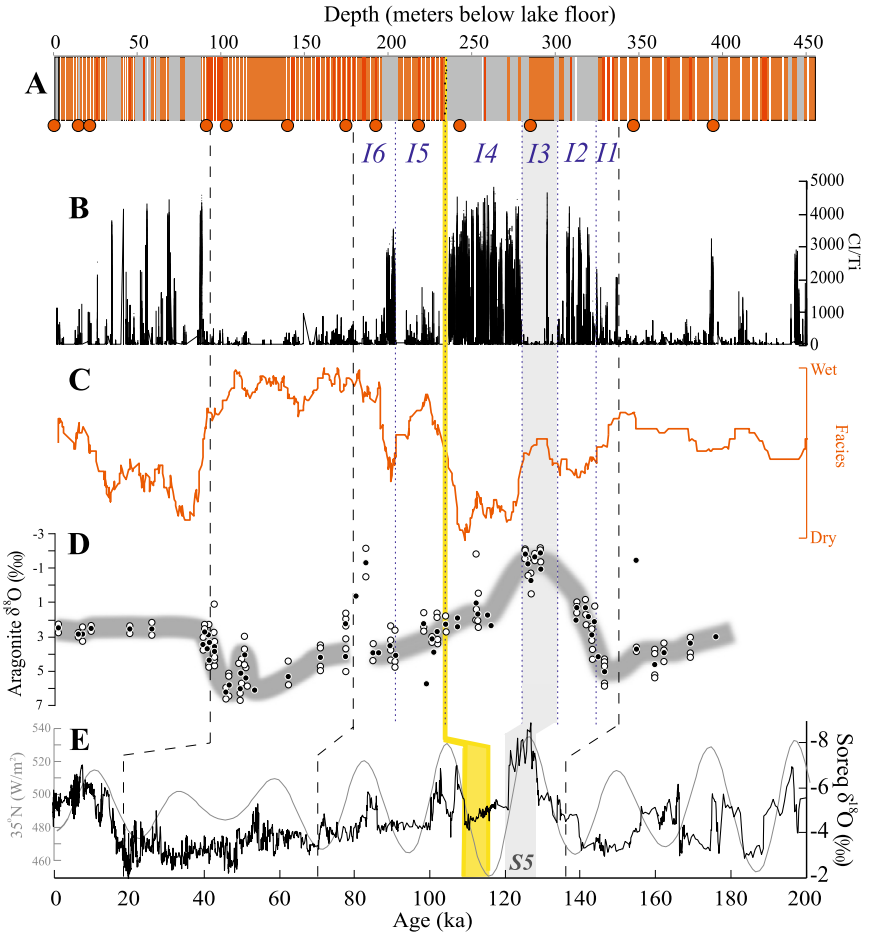

Fig. 4. Compiled lithology and comparison to Soreq Cave. (A) Generalized stratigraphic column of the 456-m-thick DSDDP sequence (see Fig. 2 captions for color code). Depths of U–Th ages are marked by red circles. *I1–I6* mark the last interglacial stratigraphic intervals, (B) XRF Cl/Ti ratios, highlighting halite rich (high Cl/Ti) compared to silt (low Cl/Ti) intervals. The halite appears in well-defined intervals, whose ages correspond to interglacials, (C) A running curve of lithological facies in the core reflects varying limnologic–climatic conditions, ranging between *aad* intervals, through laminated and massive marls, gypsum and fine sand, to sand, pebbles and halite, reflecting wet, intermediate, arid, and hyperarid climate conditions, respectively (details in Supplementary Material). (D) δ^{18}O of aragonite laminae (black circles-individual sample values; white circles-average values). Combined with U–Th ages, the smoothed (gray) curve, and lithological facies, the stratigraphy is tied to (E) the chronology and δ^{18}O record of Soreq Cave, located ~60 km west of the Dead Sea (data for 0–160 ka from Grant et al. (2012); 160–200 ka from Bar-Matthews et al. (2003), where the 177–200 ka interval is based on the Peqi'in Cave record). A gray vertical band marks the timing of sapropel S5 and concurrent *I*-3 interval in the DSDDP core. A thin yellow band at ~235 m marks a 40-cm thick pebble layer that caps the massive *I-4* halite sequence, together marking a unique drawdown of Dead Sea levels and a sedimentary hiatus between ~116–110 ka. (For interpretation of the references to color in this figure legend, the reader is referred to the web version of this article.)

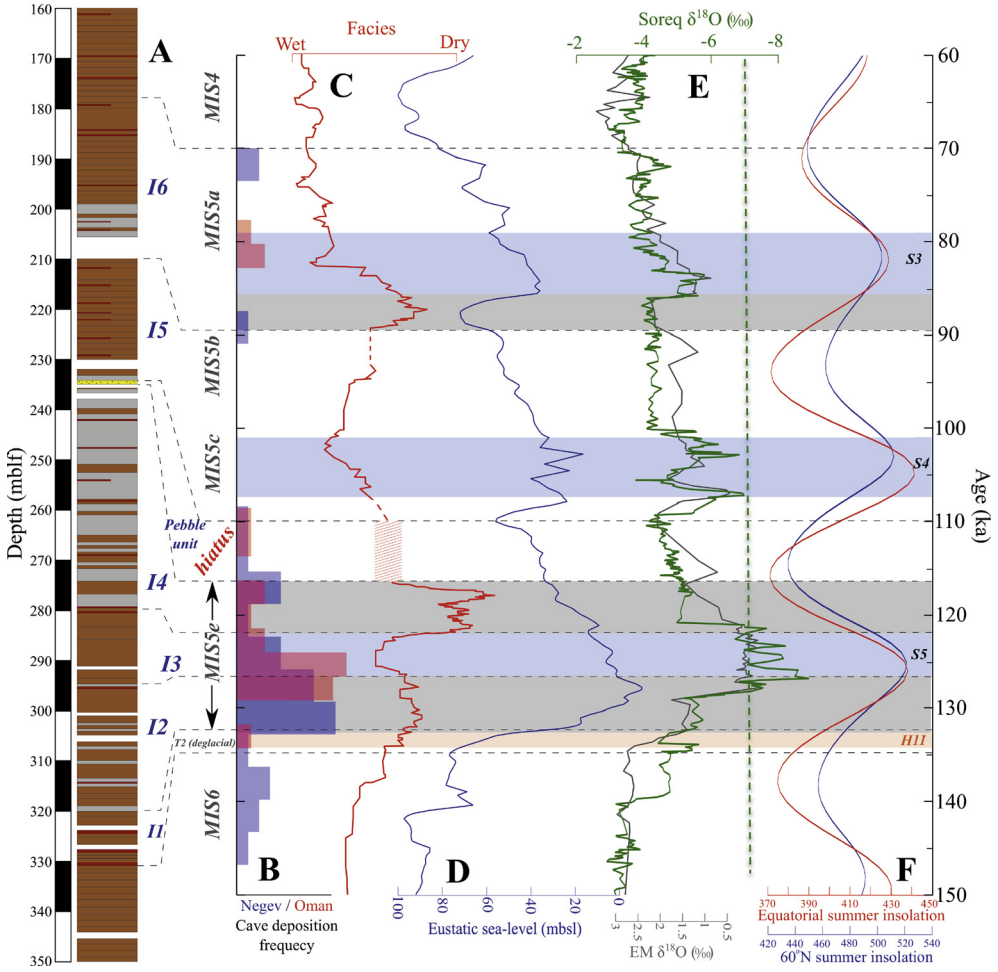

Fig. 5. MIS5 in the DSDDP core and other records. (A) Stratigraphic column of MIS5, (B) Frequency of cave deposits in the southern and central Negev (Vaks et al., 2007) and southern Arabian Peninsula (Hoti Cave, Fleitmann et al., 2003), showing a prominent peak coinciding *I*-3, (C) The compiled facies curve (details in Fig. 2 caption) reflects regional wetter and drier hydrological cycles, (D) Eustatic sea-level (mbsl) (Grant et al., 2012), (E) Soreq Cave δ^{18}O record (green) and East Mediterranean (EM) sediment core LC21 record for planktonic foraminifera (gray) (Grant et al., 2012). A negative δ^{18}O excursion at ~128–122 ka marks a threshold crossing (indicated by the green dashed curve) that corresponds to an exceptional intensification and northward expansion of the tropical (African monsoon) moisture sources, which occurred only during the MIS5e summer insolation peak (F). Other summer insolation peaks at ~105 and ~83 ka had a less dramatic effect though hyperarid conditions appear to have been dampened at both times (see text for details). The lake gradually recuperated from its post-MIS5e drawdown during the MIS5c and MIS5b. Grey rectangles mark the timing of halite deposition in the Dead Sea and blue rectangles mark the timing of sapropel events in the Mediterranean. (For interpretation of the references to color in this figure legend, the reader is referred to the web version of this article.)

Cave speleothems (Fig. 4), associated with sapropel S5 in the Eastern Mediterranean (Bar-Matthews et al., 2003). The sapropel reflects extremely high Nile flow, caused by the unusually strong African monsoon associated with high equatorial summer insolation (Rohling et al., 2002; Rossignol-Strick, 1985). Like the Soreq speleothems, the aragonite laminae from the *I*-3 interval show extremely low δ^{18}O values (between −2 and 0‰), lower than any other time interval in the Dead Sea record, including the Holocene (Fig. 4).

Interval I-4 (~280–235 mblf, ~122–116 ka) marks the most extreme arid spell known in the Dead Sea. This time interval coincides with the waning of the African monsoon during the latter part of MIS5e. Halite dominates over ~45 m of section with thin interspersed silt and gypsum. This exceptionally long halite-dominated interval is capped by a ~40 cm thick pebble layer (at 235 mblf; Figs. 4, 5), whose appearance is similar to beach deposits along the modern Dead Sea shores (Fig. S2), suggesting its potential association with a paleo-shoreline. Together, the halite and pebble units represent a sequence of evaporation and lake level drop to below the paleo-elevation of the core site, in the deepest basin of the Dead Sea. In turn this suggests a major drawdown of the lake level at the end of MIS5e, which is supported by a ~6–7 kyr sedimentary hiatus in the DSDDP record (Fig. 3, Table 2).

Interval I-5 (~234–210 mblf, ~110–93 ka), lies above the pebble unit and comprises a ~20 m thick sequence of silt sediments and sporadic gypsum layers. This unit marks resumed wetness and gradual recovery of the lake level during MIS 5c and 5b, coeval with sapropel event S4 in the Mediterranean, though the African monsoon, considered a potential driver of moisture delivery to the East Mediterranean–Levant region, was apparently weak during this time interval, as indicated by the gaps in several other regional records (Figs. 5, 7).

Interval I-6 (~206–177 mblf ~90–70 ka) marks a return to hyperaridity during the transition into MIS5a, represented by halite and intermittent gypsum and silt. Subsequently, during the rest of MIS5a, a silt interval indicates more moderate conditions, possibly supported by a brief resumption intensified African monsoon activity (coinciding with S3 in the East Mediterranean; Rossignol-Strick, 1985), and the re-appearance of an *aad*-dominated sequence marks the onset of the last glacial cycle and the transition to the Lisan Formation.

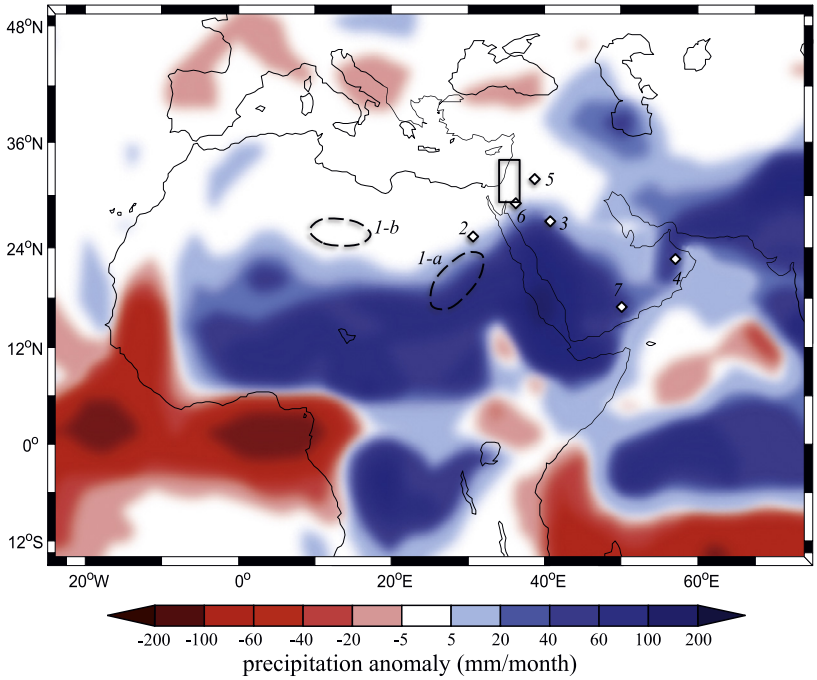

Fig. 6. Climate model simulation (expressed as Eemian minus pre-industrial) for summer precipitation (in mm/month) (Modified after Herold and Lohmann, 2009). Blue areas mark the location of sites where excess precipitation has been identified during the last interglacial, and red areas mark the location of sites that experienced arid conditions during these times. Location of sites in North Africa, Arabia and the Levant that are discussed in this paper: (1a) Szabo et al. (1995); Smith et al. (2007); (1b) Geyh and Thiedig (2008); (2) Crombie et al. (1997); (3) Rosenberg et al. (2013); (4) Fleitmann et al. (2003); (5) Azraq Oasis–Jordan (Cordova et al., 2013); (6) South Jordan (Petit-Maire et al., 2010); (7) Yemen Cave (Fleitmann et al., 2011). The northern part of the Dead Sea watershed is dominated by sub-tropical Mediterranean climate, while the southern part, around the hypersaline Dead Sea and southwards, is dominated by Saharo–Arabian desert climate (marked by black rectangle; see also Fig. 1). Minor changes in the gradient between these climate zones impose significant changes in the hydrological budget of the Dead Sea basin. (For interpretation of the references to color in this figure legend, the reader is referred to the web version of this article.)

5. Climate control on the East Mediterranean–Levant hydrology

The *DSDDP* sedimentary column provides a surprising perspective on the last interglacial climate in the Levant. Based on the long term relationships between sedimentary facies and climate in the Dead Sea basin, a more arid-related sediment facies (halite, gypsum and silt) would be expected to dominate during NH summer insolation maxima (MIS 5a, c, e) and wetter facies (silt and aad) during summer insolation minima (MIS5b, d). Accordingly, the MIS5e interglacial peak at ~128–122 ka is expected to reflect extreme hyperarid conditions. Yet, the DSDDP stratigraphy shows that the MIS5e insolation peak is coincident with relative wetness in the Levant, which is also coeval with the S5 sapropel in the Mediterranean, it self associated with an intensification of the African monsoon.

The identification of the source of the MIS5e moisture to the Dead Sea watershed poses a perplexing question. The Mediterranean sapropel layers are considered to be the result of enhanced Nile River flow, fed by the remote precipitation increase in low latitudes, associated with an intense African summer monsoon (Rohling et al., 2002; Rossignol-Strick, 1985). Yet, the ability of monsoon-related southern-derived rains to directly impact the Dead Sea watershed is not trivial, considering the relatively high latitude of the lake and the distance from tropical Africa. However, a significant northern excursion of summer monsoon rainfall is displayed in recent general circulation models (e.g., Herold and Lohmann, 2009), suggesting that the African monsoon influence could have reached as far north as the northern Arabian Peninsula and the southern end of the Dead Sea watershed, triggering summer rains of up to ~30–60 mm per summer (Fig. 6). It should also be noted that in recent years, the most significant floods in the southern Negev–Arava are the result of rainstorms associated with "tropical moisture plumes" crossing north Africa and impacting the deserts of the Middle East (Kahana et al., 2002; Rubin et al., 2007; Ziv, 2001). These storms can therefore provide an indication of an alternative, or complementary, efficient mechanism for the impact of southern sources of humidity on the Dead Sea watershed. Because of their localized impact however, they are not necessarily associated with a regional scale north-south geographic trend, as indicated from their modern input in Sinai, Negev, Jordan, and NW Arabia deserts (Rubin et al., 2007). Our hypothesis that southern rainfall sources affected the Dead Sea watershed during the MIS5e peak is corroborated by other regional hydroclimate archives (Figs. 1, 6, 7) such as southern Negev Desert speleothems (Vaks et al., 2010, 2007), travertine-spring deposits in the Arava valley (Livnat and Kronfeld, 1985; Waldmann et al., 2010), and MIS5e ages of calcification processes in the Red Sea coral reefs indicating enhanced coastal fresh groundwater activity in the currently hyperarid Gulf of Aqaba (Lazar and Stein, 2011). The evidence from the Negev–Arava–Red Sea archives are supported by additional evidence from cave deposits in the southern Arabian Peninsula (Fleitmann et al., 2011, 2003), and spring and possibly lacustrine or groundwater overflow deposits in Northern and Eastern Sahara (Geyh and Thiedig, 2008; McKenzie, 1993; Szabo et al., 1995), Arabia (Rosenberg et al., 2013), and south Jordan (Petit-Maire et al., 2010; note however, a revised evaluation of the latter by Catlett, 2014). Collectively, these observations indicate that tropical-derived precipitation could have reached as far north as the Dead Sea watershed during MIS5e, inverting the common hyperaridy persisting during full interglacials. As a result, the Dead Sea system was maintained above the annual hydrologic threshold of halite precipitation through the MIS5e peak, as reflected by core interval *I-3*. The collapse of the hydrological system was therefore postponed for several thousand years, until the effect of the southern humidity sources weakened (Fig. 5b), and the annual inflow to the lake fell below the threshold of halite precipitation.

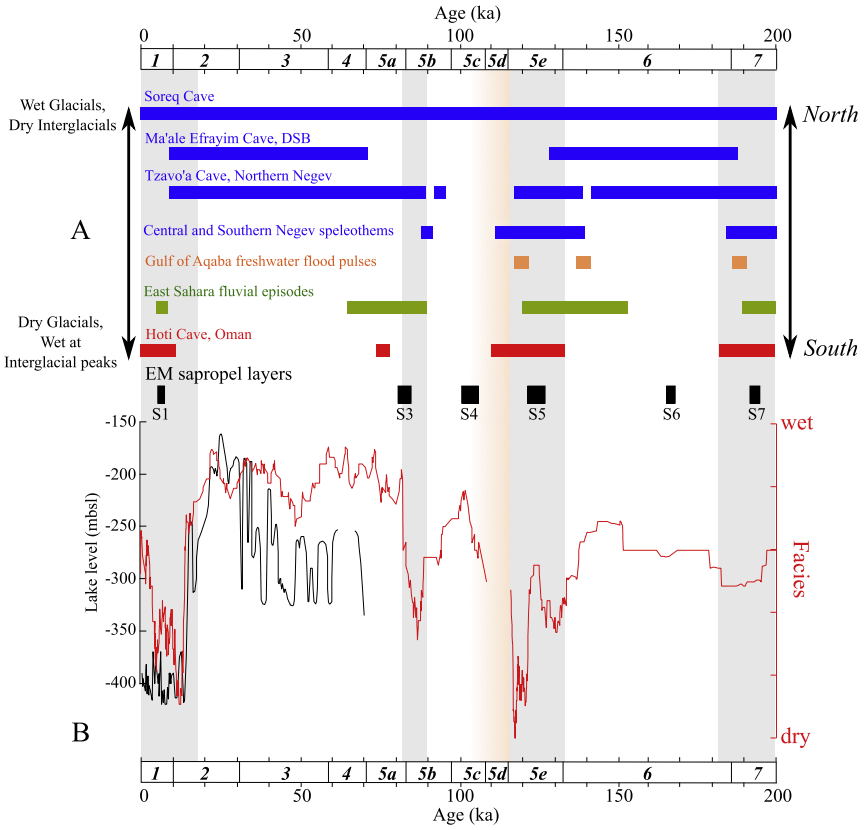

Fig. 7. (A) Comparison to Middle Eastern climate archives over the last 200 kyrs. The Soreq Cave displays continuous deposition reflecting the dominance of NH-Mediterranean climate systems during most of this time interval (Bar-Matthews et al., 2003; Grant et al., 2012). In contrast, cave deposits in the desert's margins (e.g., northern Negev Desert (Vaks et al., 2007, 2006) and central Dead Sea watershed (Vaks et al., 2003)) were active only during glacials (similarly, the Azraq Oasis in Jordan appears to have recorded wet conditions during glacial times; Cordova et al., 2013) while caves in the southern Negev Desert (Vaks et al., 2007) and the Arabian Peninsula (Fleitmann et al., 2003) were active only during interglacials. Similarly, although their timing is not as well constrained, wetter conditions occurred during interglacials in the Sahara (Szabo et al., 1995) and along the Gulf of Aqaba (Lazar and Stein, 2011). The timing of sapropel (S) events is after Bar-Matthews et al. (2003). A light-orange band at ~116–110 ka marks the sedimentary hiatus in the core, which corresponds to a similar hiatus in records located south and east of the Soreq Cave. Grey rectangles mark the timing of salt deposition in the core. (B) The age normalized facies curve (red) for the DSDDP core and Dead Sea level reconstruction of the past 70 kyrs (black; Torfstein et al., 2013b). The curves show good overlap, indicating that the facies curve is a robust recorder of lake conditions. (For interpretation of the references to color in this figure legend, the reader is referred to the web version of this article.)

An effective incursion of tropic-derived precipitation systems as far north as the southern Dead Sea watershed must have been limited to the peak of MIS5e (~128–122 ka, coeval with sapropel S5 and DSDDP *Interval I-3*). Indeed, the S5-associated wet anomaly is well documented in both the DSDDP core and Soreq Cave, where the lightest $\delta^{18}O$ values are recorded in both archives (Figs. 4, 5). Because the main source of precipitation in the Levant is the Eastern Mediterranean, both records show a remarkably similar variability in $\delta^{18}O$ values, following the pattern of East Mediterranean planktonic foraminifera $\delta^{18}O$ (Kolodny et al., 2005). During the peak of MIS5e, the enhanced freshwater inflow, which was delivered to the Mediterranean primarily by the Nile River and to a lesser extent to the southern Levant by southern rain, imposed uniquely low $\delta^{18}O$ values that stem from the input of far traveled precipitation.

The African monsoon contribution to Arabia declined gradually from the MIS5e peak until ~110 ka, when it became negligible, as expressed by the declining frequency of cave deposits in Oman (Fleitmann et al., 2003) and in the Negev Desert (Vaks et al., 2007, 2006) (Fig. 5b). This resulted in a significant lake drop and a major phase of salt deposition, as reflected in the *I-4* core interval and the sedimentary hiatus that follows it, between ~116–110 ka. This lake-level drop marks one of them most extreme regional aridity cycles associated with the combined effect of a NH-dominated hyperarid interglacial, a weakening African monsoon, and the already moisture-deprived hydrological system of the Dead Sea watershed.

Recovery of the Dead Sea watershed from hyperarid conditions might be expected during MIS5d (~116–110 ka), which is considered less extreme than MIS5e. Yet the hydrological system was still water-deprived and lake levels remained extremely low. Following the shift into MIS5c ca. 110 ka, the DSDDP record displays renewed deposition of silt and gypsum beds, indicating a limited and gradual recovery of the hydrological system. It should be noted that spring and cave deposits in the Saharo–Arabian area generally ceased forming during this time interval (Fig. 7), reflecting continued hyperarid conditions. Thereafter, the gradual recovery continued through MIS5b, when global and regional climate conditions became more moderate, but terminated abruptly with the deposition of massive halite ca. ~90–85 ka (206–199 mblf). This arid spell was followed by relatively moderate conditions that could be related to the combination of a resumed, albeit brief, contribution of the southern rains during the peak of MIS5a (~85–80 ka), coinciding with sapropel S3 in the Mediterranean (Grant et al., 2012; Rossignol-Strick, 1985), and the gradual NH shift toward the MIS4 glacial stage, which imposed much wetter conditions in the Dead Sea watershed.

6. Summary and conclusions

Recent drilling by the Dead Sea Deep Drilling Project in the deepest basin of the hypersaline Dead Sea at ~723 mbsl recovered

sediment cores that record the late Quaternary limnological history of the lake and the hydro-climatic history of its watershed between the present day and MIS7 at ~200 ka. This study focuses on the last interglacial period (MIS5), including new observations regarding the impacts of particularly intense precession-driven monsoons at the mid subtropical latitude of the Dead Sea watershed.

Relative wetness is reflected by sequences of alternating aragonite and silty laminae (*aad* facies), and increasing aridity is reflected by decreasing amounts of aragonite and a corresponding increase in the content of laminated detritus (*ld* facies), then gypsum, then halite. The chronology of the DSDDP core has been established by integration of U–Th ages of primary aragonite, $\delta^{18}O$ oxygen isotope stratigraphy and comparison of the main lithological units to regional and global archives. The chronostratigraphy shows that the *aad* facies is largely associated with glacials, while halite deposition marks regional aridity and lake drops uniquely associated with interglacials.

The sediment sequence deposited in the Dead Sea during MIS5 records the interplay between the effects of NH climate and intense precession driven African moisture sources on the climate of the Eastern Mediterranean–Levant corridor. The NH climatology imposes arid interglacials and wetter glacials in the region, while particularly intense African monsoons, such as the one that generated sapropel S5 in the Eastern Mediterranean during the peak of MIS5e, moderated the aridity otherwise expected in the Dead Sea basin. The new findings confirm that in the absence of these tropical effects, the Levant corridor would have been extremely hyperarid during MIS5e, leading to an early catastrophic drop of the Dead Sea. Instead, a major lake drawdown took place during the late stages of MIS5e.

In the context of human prehistory, wetness in the region coeval with an intensified African monsoon may have facilitated hominid migration out of Africa (e.g., Frumkin et al., 2011; Lazar and Stein, 2011; Vaks et al., 2007; Waldmann et al., 2010; Walter et al., 2000), while otherwise a regional climate barrier of aridity persisted across the Levant, Arabia and Eastern Sahara during much of MIS5. Finally, the findings reported here support general circulation model results (e.g., Held and Soden, 2006) predicting that warmer mean global temperatures may exacerbate an important resource problem by causing a decline in Levant fresh water availability.

Acknowledgements

We acknowledge the International Continental Scientific Drilling Foundation (ICDP), Israel Science Foundation (ISF), and US NSF (grant EAR 11-15312 to SLG and Emi Ito) for funding the coring, and DOSECC (Drilling, Observation and Sampling of the Earth's Continental Crust) for performing the drilling operation. The cores were opened and described by a large team under the auspices of the Professor A. Brauer at GFZ-Potsdam. We wish to thank the many participants who took part in the drilling operations, core opening and sampling. Rachel Lupien carefully separated and prepared aragonite laminae for oxygen isotope analyses. The scientific study is supported by the Comer Science & Education Foundation (grant #CP69 to AT), the USA–Israel Bi-National Science Foundation (BSF, grant #2010375 to SLG and MS), the Dead Sea Drill Excellence Center of the Israel Science Foundation (grant # 1736/11 to YE, Boaz Lazar, and Yigal Erel), the National Oceanic and Atmospheric Administration (grant NA10OAR4320137 to YK), and the Storke Endowment at Columbia University (to SLG). This is Dead Sea Excellence Center contribution #4 and LDEO contribution #7849. Two anonymous reviewers are thanked for providing helpful and constructive comments.

Appendix A. Supplementary material

Supplementary material related to this article can be found online at http://dx.doi.org/10.1016/j.epsl.2014.12.013.

References

Bar-Matthews, M., 2014. History of water in the Middle East and North Africa. In: Archaeology and Anthropology. Elsevier Ltd., pp. 109–128.
Bar-Matthews, M., Ayalon, A., Gilmour, M., Matthews, A., Hawksworth, C.J., 2003. Sea–land oxygen isotopic relationships from planktonic foraminifera and speleothems in the Eastern Mediterranean region and their implication for paleorainfall during. Geochim. Cosmochim. Acta 67, 3181–3199.
Bartov, Y., Stein, M., Enzel, Y., Agnon, A., Reches, Z., 2002. Lake levels and sequence stratigraphy of lake Lisan, the late Pleistocene precursor of the Dead Sea. Quat. Res. 57, 9–21.
Bartov, Y., Goldstein, S.L., Stein, M., Enzel, Y., 2003. Catastrophic arid episodes in the Eastern Mediterranean linked with the North Atlantic Heinrich events. Geology 31, 439–442.
Begin, Z., Ehrlich, A., Nathan, Y., 1974. Lake Lisan, the Pleistocene precursor of the Dead Sea. Geol. Surv. Isr. Bull. 63, 1–30.
Bookman (Ken-Tor), R., Enzel, Y., Agnon, A., Stein, M., 2004. Late Holocene lake levels of the Dead Sea. Geol. Soc. Am. Bull. 116, 555.
Catlett, G.A., 2014. Pluvial deposits in Mudawwara, Jordan and their implications for Mediterranean and monsoonal precipitation in the Levant. MSc thesis. Miami University.
Cordova, C.E., Nowell, A., Bisson, M., Ames, C.J.H., Pokines, J., Chang, M., al-Nahar, M., 2013. Interglacial and glacial desert refugia and the Middle Paleolithic of the Azraq Oasis, Jordan. Quat. Int. 300, 94–110.
Crombie, M.K., Arvidson, R.E., Sturchio, N.C., El Alfy, Z., Zeid, K.A., 1997. Age and isotopic constraints on Pleistocene pluvial episodes in the Western Desert, Egypt. Palaeogeogr. Palaeoclimatol. Palaeoecol. 130, 337–355.
Enzel, Y., Amit, R., Dayan, U., Crouvi, O., Kahana, R., Ziv, B., Sharon, D., 2008. The climatic and physiographic controls of the eastern Mediterranean over the late Pleistocene climates in the southern Levant and its neighboring deserts. Glob. Planet. Change 60, 165–192.
Fleitmann, D., Burns, S.J., Neff, U., Mangini, A., Matter, A., 2003. Changing moisture sources over the last 330,000 years in Northern Oman from fluid-inclusion evidence in speleothems. Quat. Res. 60, 223–232.
Fleitmann, D., Burns, S.J., Pekala, M., Mangini, A., Al-Subbary, A., Al-Aowah, M., Kramers, J., Matter, A., 2011. Holocene and Pleistocene pluvial periods in Yemen, southern Arabia. Quat. Sci. Rev. 30, 783–787.
Frumkin, A., Bar-Yosef, O., Schwarcz, H.P., 2011. Possible paleohydrologic and paleoclimatic effects on hominin migration and occupation of the Levantine Middle Paleolithic. J. Hum. Evol. 60, 437–451.
Geyh, M.A., Thiedig, F., 2008. The Middle Pleistocene Al Mahrúqah Formation in the Murzuq Basin, northern Sahara, Libya evidence for orbitally-forced humid episodes during the last 500,000 years. Palaeogeogr. Palaeoclimatol. Palaeoecol. 257, 1–21.
Grant, K.M., Rohling, E.J., Bar-Matthews, M., Ayalon, A., Medina-Elizalde, M., Bronk Ramsey, C., Satow, C., Roberts, A.P., 2012. Rapid coupling between ice volume and polar temperature over the past 150,000 years. Nature 491, 744–747.
Haase-Schramm, A., Goldstein, S.L., Stein, M., 2004. U–Th dating of Lake Lisan (late Pleistocene dead sea) aragonite and implications for glacial east Mediterranean climate change. Geochim. Cosmochim. Acta 68, 985–1005.
Haliva-Cohen, A., Stein, M., Goldstein, S.L., Sandler, A., Starinsky, A., 2012. Sources and transport routes of fine detritus material to the Late Quaternary Dead Sea basin. Quat. Sci. Rev. 50, 55–70.
Held, I., Soden, B., 2006. Robust responses of the hydrological cycle to global warming. J. Climate 19, 5686–5699.
Hemming, S., 2004. Heinrich events: massive late Pleistocene detritus layers of the North Atlantic and their global imprint. Rev. Geophys. 42, 2003RG000128.
Herold, M., Lohmann, G., 2009. Eemian tropical and subtropical African moisture transport: an isotope modelling study. Clim. Dyn. 33, 1075–1088.
Kahana, R., Ziv, B., Enzel, Y., Dayan, U., 2002. Synoptic climatology of major floods in the Negev Desert, Israel. Int. J. Climatol. 22, 867–882.
Kaufman, A., 1971. U-Series dating of Dead Sea Basin carbonates. Geochim. Cosmochim. Acta 35, 1269–1281.
Kaufman, A., Yechieli, Y., Gardosh, M., 1992. Reevaluation of the lake-sediment chronology in the Dead Sea basin, Israel, based on new $^{230}Th/U$ dates. Quat. Res. 304, 292–304.
Kolodny, Y., Stein, M., Machlus, M., 2005. Sea-rain-lake relation in the Last Glacial East Mediterranean revealed by $\delta^{18}O$–$\delta^{13}C$ in Lake Lisan aragonites. Geochim. Cosmochim. Acta 69, 4045–4060.
Kushnir, Y., Stein, M., 2010. North Atlantic influence on 19th–20th century rainfall in the Dead Sea watershed, teleconnections with the Sahel, and implication for Holocene climate fluctuations. Quat. Sci. Rev. 29, 3843–3860.
Lazar, B., Stein, M., 2011. Freshwater on the route of hominids out of Africa revealed by U–Th in Red Sea corals. Geology 39, 1067–1070.

Lisiecki, L.E., Raymo, M.E., 2005. A Pliocene–Pleistocene stack of 57 globally distributed benthic $\delta^{18}O$ records. Paleoceanography 20, PA1003.
Livnat, A., Kronfeld, J., 1985. Paleoclimatic implications of U-series dates for lake sediments and travertines in the Arava Rift Valley, Israel. Quat. Res. 24, 164–172.
McKenzie, J.a., 1993. Pluvial conditions in the eastern Sahara following the penultimate deglaciation: implications for changes in atmospheric circulation patterns with global warming. Palaeogeogr. Palaeoclimatol. Palaeoecol. 103, 95–105.
Migowski, C., Stein, M., Prasad, S., Negendank, J.F.W., Agnon, A., 2006. Holocene climate variability and cultural evolution in the Near East from the Dead Sea sedimentary record. Quat. Res. 66, 421–431.
Neev, D., Emery, K.O., 1967. The Dead Sea, depositional processes and environments of evaporites. Geol. Surv. Isr. Bull. 41, 147 pp.
Neugebauer, I., Brauer, A., Schwab, M.J., Waldmann, N., Enzel, Y., Kitagawa, H., Torfstein, A., Frank, U., Dulski, P., Agnon, A., Ariztegui, D., Ben-Avraham, Z., Goldstein, S.L., Stein, M., 2014. Lithology of the long sediment record recovered by the ICDP Dead Sea Deep Drilling Project (DSDDP). Quat. Sci. Rev. 102, 149–165.
Petit-Maire, N., Carbonel, P., Reyss, J.L., Sanlaville, P., Abed, a., Bourrouilh, R., Fontugne, M., Yasin, S., 2010. A vast Eemian palaeolake in Southern Jordan (29°N). Glob. Planet. Change 72, 368–373.
Prasad, S., Vos, H., Negendank, J.F.W., Waldmann, N., Goldstein, S.L., Stein, M., 2004. Evidence from Lake Lisan of solar influence on decadal- to centennial-scale climate variability during marine oxygen isotope stage 2. Geology 32, 581.
Rohling, E.J., Cane, T.R., Cooke, S., Sprovieri, M., Bouloubassi, I., Emeis, K.C., Schiebel, R., Kroon, D., Jorissen, F.J., Lorre, a., Kemp a, E.S., 2002. African monsoon variability during the previous interglacial maximum. Earth Planet. Sci. Lett. 202, 61–75.
Rosenberg, T.M., Preusser, F., Risberg, J., Plikk, A., Kadi, K.A., Matter, A., Fleitmann, D., 2013. Middle and Late Pleistocene humid periods recorded in palaeolake deposits of the Nafud desert, Saudi Arabia. Quat. Sci. Rev. 70, 109–123.
Rossignol-Strick, M., 1985. Mediterranean Quaternary sapropels, an immediate response of the African monsoon to variation of insolation. Palaeogeogr. Palaeoclimatol. Palaeoecol. 49, 237–263.
Rubin, S., Ziv, B., Paldor, N., 2007. Tropical plumes over Eastern North Africa as a Source of rain in the Middle East. Mon. Weather Rev. 135, 4135–4148.
Schramm, A., Stein, M., Goldstein, S., 2000. Calibration of the 14°C time scale to >40 ka by ^{234}U– ^{230}Th dating of Lake Lisan sediments (last glacial Dead Sea). Earth Planet. Sci. Lett. 175, 27–40.
Smith, J.R., Hawkins, A.L., Asmerom, Y., Polyak, V., Giegengack, R., 2007. New age constraints on the Middle Stone Age occupations of Kharga Oasis, Western Desert, Egypt. J. Hum. Evol. 52, 690–701.
Stein, M., 2001. The sedimentary and geochemical record of Neogene-Quaternary water bodies in the Dead Sea Basin – inferences for the regional paleoclimatic history. J. Paleolimnol. 26, 271–282.
Stein, M., Starinsky, A., Katz, A., Goldstein, S.L., Machlus, M., Schramm, A., 1997. Strontium isotopic, chemical, and sedimentological evidence for the evolution of Lake Lisan and the Dead Sea. Geochim. Cosmochim. Acta 61, 3875–3992.
Stein, M., Torfstein, A., Gavrieli, I., Yechieli, Y., 2010. Abrupt aridities and salt deposition in the post-glacial Dead Sea and their North Atlantic connection. Quat. Sci. Rev. 29, 567–575.
Szabo, B., Haynes, C., Maxwell, T., 1995. Ages of Quaternary pluvial episodes determined by uranium-series and radiocarbon dating of lacustrine deposits of Eastern Sahara. Palaeogeogr. Palaeoclimatol. Palaeoecol. 113, 227–242.
Torfstein, A., Gavrieli, I., Stein, M., 2005. The sources and evolution of sulfur in the hypersaline Lake Lisan (paleo-Dead Sea). Earth Planet. Sci. Lett. 236, 61–77.
Torfstein, A., Gavrieli, I., Katz, A., Kolodny, Y., Stein, M., 2008. Gypsum as a monitor of the paleo-limnological–hydrological conditions in Lake Lisan and the Dead Sea. Geochim. Cosmochim. Acta 72, 2491–2509.
Torfstein, A., Haase-Schramm, A., Waldmann, N., Kolodny, Y., Stein, M., 2009. U-series and oxygen isotope chronology of the mid-Pleistocene Lake Amora (Dead Sea basin). Geochim. Cosmochim. Acta 73, 2603–2630.
Torfstein, A., Goldstein, S., Kagan, E.J., Stein, M., 2013a. Integrated multi-site U–Th chronology of the last glacial Lake Lisan. Geochim. Cosmochim. Acta 104, 210–231.
Torfstein, A., Goldstein, S., Stein, M., Enzel, Y., 2013b. Impacts of abrupt climate changes in the Levant from Last Glacial Dead Sea levels. Quat. Sci. Rev. 69, 1–7.
Vaks, A., Bar-Matthews, M., Ayalon, A., Schilman, B., Gilmour, M., Hawkesworth, C.J., Frumkin, A., Kaufman, A., Matthews, A., 2003. Paleoclimate reconstruction based on the timing of speleothem growth and oxygen and carbon isotope composition in a cave located in the rain shadow in Israel. Quat. Res. 59, 182–193.
Vaks, A., Bar-Matthews, M., Ayalon, A., Matthews, A., Frumkin, A., Dayan, U., Halicz, L., Almogi-Labin, A., Schilman, B., 2006. Paleoclimate and location of the border between Mediterranean climate region and the Saharo–Arabian Desert as revealed by speleothems from the northern Negev Desert, Israel. Earth Planet. Sci. Lett. 249, 384–399.
Vaks, A., Bar-Matthews, M., Ayalon, A., Matthews, A., Halicz, L., Frumkin, A., 2007. Desert speleothems reveal climatic window for African exodus of early modern humans. Geology 35, 831.
Vaks, A., Bar-Matthews, M., Matthews, A., Ayalon, A., Frumkin, A., 2010. Middle-Late Quaternary paleoclimate of northern margins of the Saharan–Arabian Desert: reconstruction from speleothems of Negev Desert, Israel. Quat. Sci. Rev. 29, 2647–2662.
Waldmann, N., Stein, M., Ariztegui, D., Starinsky, A., 2009. Stratigraphy, depositional environments and level reconstruction of the last interglacial Lake Samra in the Dead Sea basin. Quat. Res. 72, 1–15.
Waldmann, N., Torfstein, A., Stein, M., 2010. Northward intrusions of low- and mid-latitude storms across the Saharo–Arabian belt during past interglacials. Geology 38, 567–570.
Walter, R., Buffler, R., Bruggemann, J., Guillaume, M., Berhe, S., Negassi, B., Libsekal, Y., Cheng, H., Edwards, R., von Cosel, R., Neraudeau, D., Gagnon, M., 2000. Early human occupation of the Red Sea coast of Eritrea during the last interglacial. Nature 405, 65–69.
Yechieli, Y., Magaritz, M., Levy, Y., Weber, U., Kafri, U., Woelfli, W., Bonani, G., 1993. Late Quaternary geological history of the Dead Sea area, Israel. Quat. Res. 39, 59–67.
Ziv, B., 2001. A subtropical rainstorm associated with a tropical plume over Africa and the Middle-East. Theor. Appl. Climatol. 102, 91–102.
Ziv, B., Dayan, U., Kushnir, Y., Roth, C., Enzel, Y., 2006. Regional and global atmospheric patterns governing rainfall in the southern Levant. Int. J. Climatol. 26, 55–73.